AIP | Journal of Applied Physics

On applicability of the "thermalized potential" solver in simulations of the plasma flow in Hall thrusters

Jinyue Geng, Lubos Brieda, Laura Rose, and Michael Keidar

Citation: J. Appl. Phys. **114**, 103305 (2013); doi: 10.1063/1.4821018
View online: http://dx.doi.org/10.1063/1.4821018
View Table of Contents: http://jap.aip.org/resource/1/JAPIAU/v114/i10
Published by the AIP Publishing LLC.

JOURNAL OF APPLIED PHYSICS **114**, 103305 (2013)

On applicability of the "thermalized potential" solver in simulations of the plasma flow in Hall thrusters

Jinyue Geng,[1,2,a)] Lubos Brieda,[3] Laura Rose,[2] and Michael Keidar[2,b)]
[1]*School of Astronautics, Beijing University of Aeronautics and Astronautics, Beijing 100191, China*
[2]*Department of Mechanical & Aerospace Engineering, The George Washington University, Washington, District of Columbia 20052, USA*
[3]*Particle in Cell Consulting LLC, Falls Church, Virginia 22046, USA*

(Received 11 June 2013; accepted 26 August 2013; published online 13 September 2013)

In Hall thrusters, the potential distribution plays an important role in discharge processes and ion acceleration. This paper presents a 2D potential solver in the Hall thruster instead of the "thermalized potential", and compares equipotential contours solved by these two methods for different magnetic field conditions. The comparison results reveal that the expected "thermalized potential" works very well when the magnetic field is nearly uniform and electron temperature is constant along the magnetic field lines. However for the case with a highly non-uniform magnetic field or variable electron temperature along the magnetic field lines, the "thermalized potential" is not accurate. In some case with magnetic separatrix inside the thruster channel, the "thermalized potential" model cannot be applied at all. In those cases, a full 2D potential solver must be applied. Overall, this paper shows the limit of applicability of the "thermalized potential" model. © *2013 AIP Publishing LLC*. [http://dx.doi.org/10.1063/1.4821018]

I. INTRODUCTION

A Hall thruster (HT) is a propulsion device in which ions are accelerated in a quasi-neutral plasma. An electric field in the HT is sustained across the magnetic field. Because of this feature, HTs offer a much higher thrust density than other types of ion thrusters. In particular, some advanced thrusters, which possess complex magnetic field topology (complex curvature of the magnetic field lines) have a higher efficiency (~60%), a lower divergence (~±22° for krypton and ~±11° for xenon) and a longer lifetime (10 400 h) due to reduced erosion.[1–8]

In the HT discharge channel, the potential distribution plays an important role in discharge processes and ion acceleration (Fig. 1). Near the thruster exit plane, the potential drops accelerate the ions,[4] thereby produce a thrust; and the potential distribution could largely affect the plasma dynamics and plasma-wall interactions. The potential in the HT channel is governed by the magnetic field distribution in that the equipotential contours tend to parallel with the magnetic field lines. This stems from the fact that the electric field tends to be zero along magnetic field lines due to high electron mobility in this direction.[9]

In order to simplify analysis of the potential distribution in the HT, Morozov[10] introduced the so-called "thermalized potential" based on the momentum equation with the assumption of a constant electron temperature along the magnetic field line. In previous modeling works of HTs, the "thermalized potential" is usually assumed to make it possible to reduce the two dimensional calculation of the electric field to a one-dimensional problem. Indeed, this approach produces reasonably good accuracy in modeling conventional HTs.[11–13] Due to the magnetic field, the mobility value is much larger for electron transport along magnetic field lines than across them.[14] Therefore, the "thermalized potential" could be considered constant along the magnetic field lines. The modeling approach based on "thermalized potential" requires that the magnetic field lines intersect walls of the channel allowing potential calculation in a 1D manner along the centerline. However, when the curvature of magnetic field lines becomes complex, the "thermalized potential" may not accurately predict the true plasma conditions anymore. In order to address the case of a complex magnetic field topology, one needs to consider a 2D potential solver. Mikellides has introduced the Hall2De solver,[8] which treats Ohm's law in the frame of reference of the magnetic field (parallel and perpendicular components, respectively). Komurasaki utilized a 2D potential solver,[15] which calculates the coefficients parallel or perpendicular to the magnetic field lines, then multiplies the rotation matrix based on the angle of magnetic field lines relative to the axis. Both solvers are based coordinate system aligned with the magnetic field. Such approach becomes troublesome when complex magnetic topology is considered.

This paper presents a 2D potential solver, which is based on the axial direction and radial direction, instead of the "thermalized potential" in HTs. Then the comparisons between equipotential contours of the plasma potential, solved by 2D potential solver, and the "thermalized potential" for different magnetic field conditions establish the limits of applicability of the potential solver based on the "thermalized potential" model.

II. MODELING APPROACH

Based on Refs. 9 and 16, the 2D potential solver is presented. The generalized Ohm's law comes from the

[a)]Electronic mail: jinyuegeng@email.gwu.edu.
[b)]Electronic mail: keidar@gwu.edu.

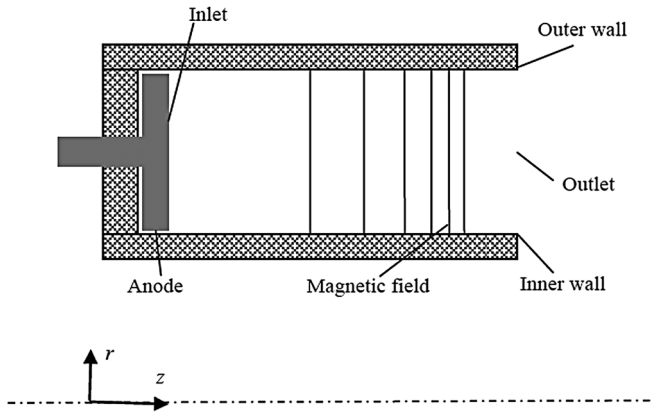

FIG. 1. Schematic drawing of the discharge channel of the Hall thruster.

momentum equation of motion for the electron fluid. It can be written as

$$\vec{E} = \frac{\vec{J}_e}{\sigma} - \frac{1}{ne}\vec{J}_e \times \vec{B} - \frac{1}{ne}\vec{\nabla}P_e, \tag{1}$$

where $\vec{J}_e$ is the electron current, P_e is the electron pressure, $\vec{B}$ is the magnetic strength, $\sigma = \mu ne$, and $\mu = e/m_e v_{ei}$. e is the elementary charge, n is the electron density, m_e is the mass of electron, and v_{ei} is the collision frequency between ions and electron. From the electron equation of state (ideal gas): $P_e = nkT_e^K = neT_e$, $\vec{\nabla}P_e = ne\vec{\nabla}T_e + eT_e\vec{\nabla}n$ is obtained (T_e^K in K unit; T_e in eV unit).

Thus, the electron current density could be obtained as the following generalized Ohm's Law formulation:

$$\vec{J}_e = \mu(\vec{J}_e \times \vec{B}) + \sigma\vec{E} + \sigma(\vec{\nabla}T_e + T_e\vec{\nabla}\ln n). \tag{2}$$

Expanding Eq. (2), a set of three equations can be written for electron current components in the axial, radial, and azimuthal directions:

$$j_z = \mu(j_\theta B_r - j_r B_\theta) + \sigma E_z + \sigma(\nabla_z T_e + T_e\nabla_z \ln n), \tag{3}$$

$$j_r = \mu(j_z B_\theta - j_\theta B_z) + \sigma E_r + \sigma(\nabla_r T_e + T_e\nabla_r \ln n), \tag{4}$$

$$j_\theta = \mu(j_r B_z - j_z B_r) + \sigma E_\theta + \sigma(\nabla_\theta T_e + T_e\nabla_\theta \ln n). \tag{5}$$

Due to the axisymmetric geometry of the HT, the electric field and gradient of the electron temperature and the plasma density in the azimuthal direction are assumed to be zero. It should be pointed out that this is simplification of the model in light of recent experiments demonstrates azimuthal spokes.[17] With this simplification, the azimuthal electron current density is no longer a function of any azimuthal quantities and it can be written as

$$j_\theta = \mu(j_r B_z - j_z B_r). \tag{6}$$

It is now possible to substitute j_θ into Eqs. (3) and (4) for the axial and radial electron current density. This leads to the following set of coupled linear equations:

$$j_z = \mu(\mu(j_r B_z - j_z B_r)B_r - j_r B_\theta) + \sigma E_z + \sigma(\nabla_z T_e + T_e\nabla_z \ln n), \tag{7}$$

$$j_r = \mu(j_z B_\theta - \mu(j_r B_z - j_z B_r)B_z) + \sigma E_r + \sigma(\nabla_r T_e + T_e\nabla_r \ln n). \tag{8}$$

This equation system can be solved to isolate the axial and the radial components of the electric current density

$$j_z = \mu_{11}\sigma(E_z + \nabla_z T_e + T_e\nabla_z \ln n) + \mu_{12}\sigma(E_r + \nabla_r T_e + T_e\nabla_r \ln n), \tag{9}$$

$$j_r = \mu_{21}\sigma(E_z + \nabla_z T_e + T_e\nabla_z \ln n) + \mu_{22}\sigma(E_r + \nabla_r T_e + T_e\nabla_r \ln n), \tag{10}$$

where

$$\mu_{11} = \frac{1+\mu^2 B_z^2}{1+\mu^2 B^2},$$

$$\mu_{12} = \frac{\mu B_\theta + \mu^2 B_z B_r}{1+\mu^2 B^2},$$

$$\mu_{21} = \frac{-\mu B_\theta + \mu^2 B_z B_r}{1+\mu^2 B^2},$$

$$\mu_{22} = \frac{1+\mu^2 B_r^2}{1+\mu^2 B^2},$$

and

$$\mu = \frac{e}{m_e v}.$$

Similarly to Ref. 11, $v = v_{en} + v_{ew} + v_B$ is the effective electron collision frequency.

The following simplifications are used to more easily manipulate the equation system:

$$j_z = Z_1 E_z + Z_2 E_r + Z_3, \tag{11}$$

$$j_r = R_1 E_z + R_2 E_r + R_3, \tag{12}$$

and

$$Z_1 = \mu_{11}\sigma,$$

$$Z_2 = \mu_{12}\sigma,$$

$$Z_3 = \mu_{11}\sigma(\nabla_z T_e + T_e\nabla_z \ln n) + \mu_{12}\sigma(\nabla_r T_e + T_e\nabla_r \ln n),$$

$$R_1 = \mu_{21}\sigma,$$

$$R_2 = \mu_{22}\sigma,$$

$$R_3 = \mu_{21}\sigma(\nabla_z T_e + T_e\nabla_z \ln n) + \mu_{22}\sigma(\nabla_r T_e + T_e\nabla_r \ln n).$$

One can employ the current conservation equation, i.e.,

$$\frac{\partial j_r}{\partial r} + \frac{\partial j_z}{\partial z} + \frac{j_r}{r} = 0. \tag{13}$$

Substitute j_z, j_r (Eqs. (11) and (12)) into Eq. (13) and using finite-difference method, one can obtain

$$(R_2^n E_r^n - R_2^s E_r^s)\cdot\Delta z + (Z_1^e E_z^e - Z_1^w E_z^w)\cdot\Delta r = S, \tag{14}$$

where

$$S = -\left[\left(R_1^n E_z^n + R_3^n\right) - \left(R_1^s E_z^s + R_3^s\right)\right] \cdot \Delta z - \left[\left(Z_2^e E_r^e + Z_3^e\right) - \left(Z_2^w E_r^w + Z_3^w\right)\right] \cdot \Delta r - \frac{1}{r}\left(R_1 E_z + R_2 E_r + R_3\right) \cdot \Delta z \cdot \Delta r.$$

The e, w, n, and s means that it is the value on the east, west, north, and south boundary of the node, respectively.

Substituting $\vec{E} = -\vec{\nabla}\varphi$ into Eq. (14), the following equation can be obtained:

$$\varphi_{i,j} = \frac{1}{Z_1^e + Z_1^w + R_2^n + R_2^s} \times \left(Z_1^e \varphi_{i+1,j} + Z_1^w \varphi_{i-1,j} + R_2^n \varphi_{i,j+1} + R_2^s \varphi_{i,j-1} - S\right). \quad (15)$$

Using Successive Over-Relaxation (SOR) method,[18] the following equation can be obtained:

$$\varphi_{i,j}^{(n+1)} = \varphi_{i,j}^{(n)} + \omega \frac{1}{Z_1^e + Z_1^w + R_2^n + R_2^s} \times \left(Z_1^e \varphi_{i+1,j}^{(n)} + Z_1^w \varphi_{i-1,j}^{(n+1)} + R_2^n \varphi_{i,j+1}^{(n)} + R_2^s \varphi_{i,j-1}^{(n+1)} - S\right); \quad (16)$$

the relaxation factor ω is 1.9 here.

III. BOUNDARY CONDITIONS

In this section, we present boundary conditions for the potential solver as well as for ion and neutral flow simulations as shown in Table I.

In Secs. V A and V B, the plasma density and temperature are assumed to be constant ($T_e = 25\,\text{eV}$; $n_e = 1 \times 10^{17}\,\text{m}^{-3}$, which are the same order of magnitude in Ref. 9, 11, and 14); in Sec. V C, the plasma density and temperature distributions are non-uniform according to plasma flow simulations.

The defined boundary conditions at the inlet and outlet are given as the thermalized potential.

IV. THERMALIZED POTENTIAL

The electron transport along magnetic field lines can be written as a balance between the pressure force and the electric force[19]

$$\vec{\nabla} P_e = -e n_e \vec{E} + m_e n_e \nu_{ei} (\vec{u}_i - \vec{u}_e), \quad (17)$$

where ν_{ei} is the electron-ion collision frequency. Because of collisionless, the second term on the right side could be neglected

$$\nabla(n_e e T_e) = e n_e \nabla\varphi, \quad (18)$$

$$\nabla T_e + \frac{T_e}{n_e} \nabla n_e = \nabla\varphi. \quad (19)$$

TABLE I. The potential boundary conditions used in the modeling.

Inlet	Outlet	Outer wall	Inner wall
Defined	Defined	$\partial\varphi/\partial r = 0$	$\partial\varphi/\partial r = 0$

So along the magnetic field lines, the following equation is given:

$$\varphi - T_e - T_e \ln n_e = const. \quad (20)$$

Since usually plasma temperature T_e is assumed constant along the magnetic field lines, a "thermalized potential" can be defined based on Eq. (18)

$$\varphi - T_e \ln n_e = const. \quad (21)$$

The left side of Eq. (21) is known as the thermalized potential. In order to make the comparisons between potential solved by 2D solver and the "thermalized potential" straightforward, the thermalized potential along the centerline of the channel is given the same value as the potential solved by 2D solver for the case in Secs. V A–V C.

V. RESULTS AND DISCUSSIONS

In this section, we describe the potential distribution in the case of various magnetic field topologies typical for HTs. In Sec. V A, a magnetic field having only radial component is considered and constant plasma density and temperature are assumed. In Sec. V B, the effect of magnetic field topology is investigated by using three different shapes of the magnetic fields assuming the uniform plasma density and temperature distribution ($T_e = 25\,\text{eV}$; $n_e = 1 \times 10^{17}\,\text{m}^{-3}$). In Sec. V C, the combined effect of magnetic field and plasma density is investigated.

The magnetic field lines, in Secs. V A and V B, are constructed using the magnetic stream function λ[20]

$$\frac{\partial\lambda}{\partial z} = r B_r, \quad (22a)$$

$$\frac{\partial\lambda}{\partial r} = -r B_z. \quad (22b)$$

A. Only radial component. Uniform plasma density and temperature

In this section, a magnetic field having only radial component is considered as shown in Fig. 2. In this calculation, uniform plasma density and temperature are assumed. The corresponded potential distribution is shown in Fig. 2(d). One can see that solution based on the 2D potential solver is almost identical to that based on the "thermalized" potential assumption. This is due to the fact that the main component of electron velocity is along the magnetic field lines, the $\vec{J}_e \times \vec{B} \to 0$.

B. Effect of the complex magnetic field topology. Uniform plasma density and temperature

In this section, three different shapes of the magnetic fields (Case 1–3) are considered, and the plasma density and temperature are constant ($T_e = 25\,\text{eV}$; $n_e = 1 \times 10^{17}\,\text{m}^{-3}$). In Figs. 3–5, (a) are the magnetic field lines; (b) are the magnetic field strengths, which are from FEMM (Finite Element Method Magnetics) simulations, respectively; (c) is the

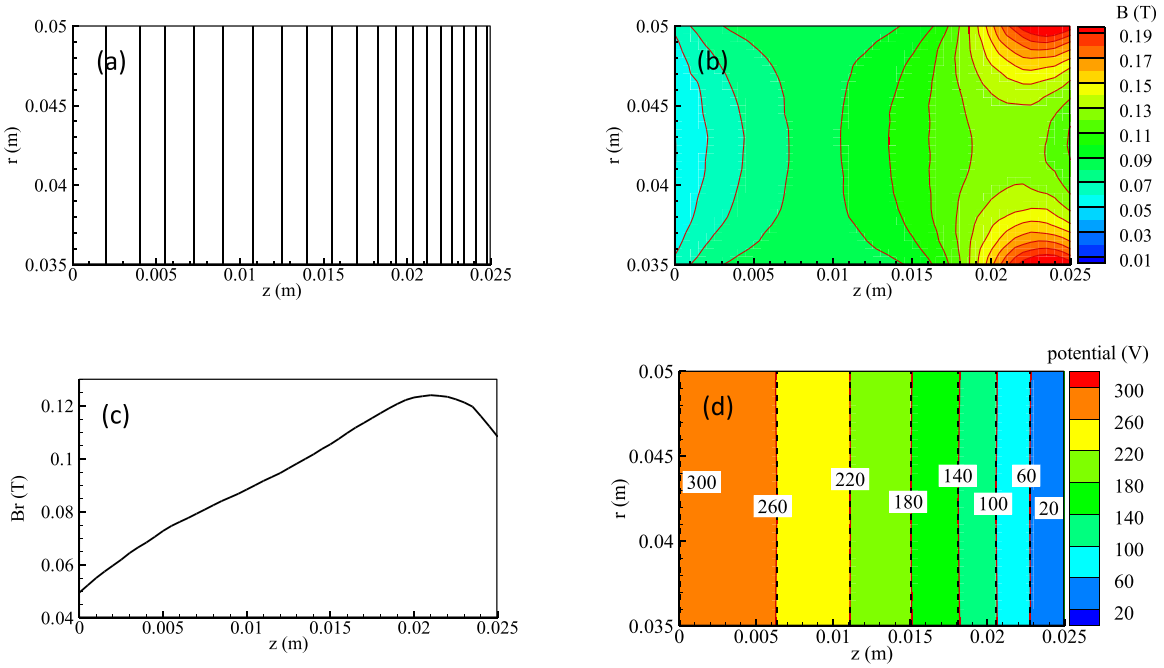

FIG. 2. Magnetic field and plasma potential distribution: (a) magnetic field lines, (b) magnetic field strength (unit: T), (c) Br along the channel centerline, (d) comparison of equipotential contours of plasma potential with "thermalized potential" (black dashed lines).

radial magnetic component along the channel centerline; and (d) is the comparison of the equipotential contours of plasma potential with "thermalized potential" (black dashed lines). FEMM,[21] is a user-friendly magnetic field solver available on the internet for solving 2D planar and axisymmetric magnetic field problems.

Results shown in Fig. 3 are based on the simulation for the uniform magnetic field (Case 1). In the entire domain, the equipotential contours of plasma potential and "thermalized potential" are close to each other, but the near wall part. The reason is that in the near wall region, the $\vec{J}_e \times \vec{B}$ term is not zero, which has been neglected in the "thermalized potential."

Results shown in Fig. 4 are based on the simulation for the magnetic field (Case 2). One can see that in this case, the equipotential contours of plasma potential and "thermalized potential" are close to each other near the outlet of the HT channel, but there are significant discrepancies in the near anode region.

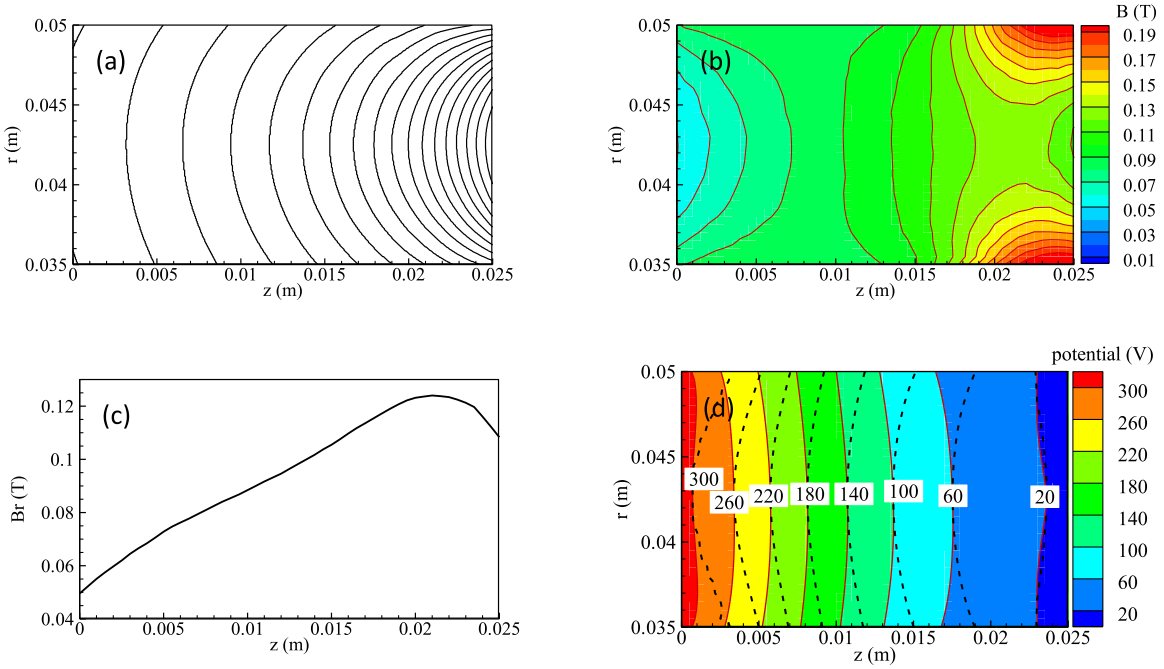

FIG. 3. Magnetic field and plasma potential distribution (Case 1): (a) magnetic field lines (Case 1), (b) magnetic field strength (unit: T), (c) Br along the channel centerline (Case 1), (d) comparison of equipotential contours of plasma potential with "thermalized potential" (black dashed lines).

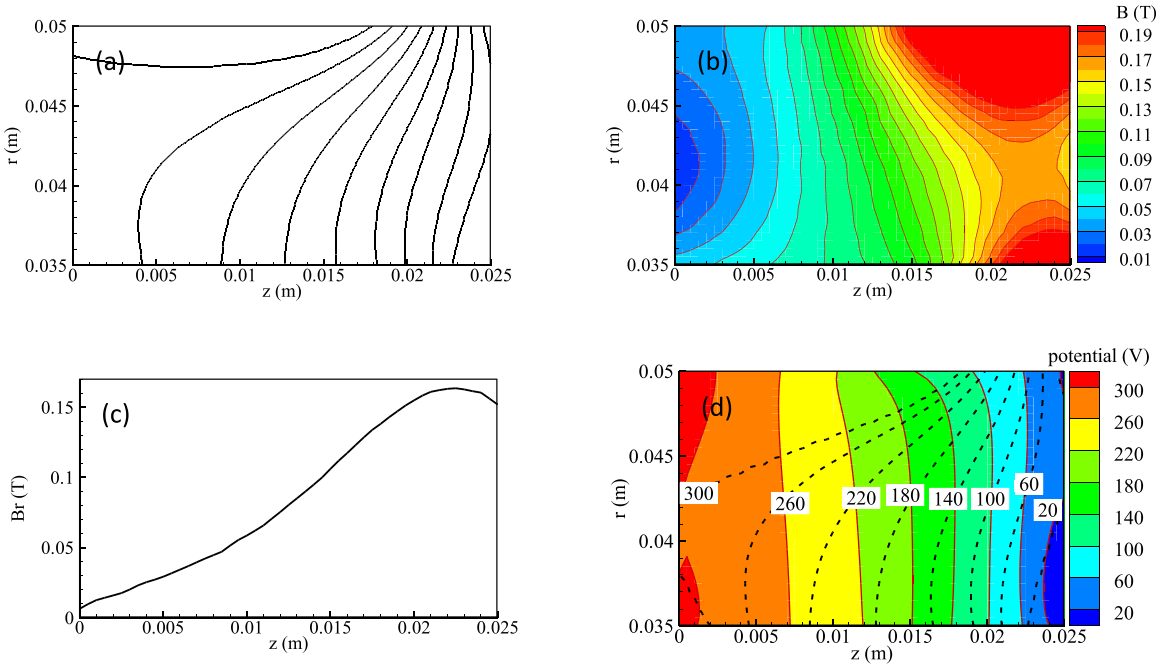

FIG. 4. Magnetic field and plasma potential distribution (Case 2): (a) magnetic field lines (Case 2), (b) magnetic field strength (unit: T), (c) Br along the channel centerline (Case 2), (d) comparison of equipotential contours of plasma potential with "thermalized potential" (black dashed lines).

Results of potential calculation for the case of a complex magnetic field (Case 3) are shown in Fig. 5. It can be seen that the equipotential contours calculated using the considered solver and the potential calculated based on the "thermalized potential" are significantly different in shape and magnitude especially in the region of low magnetic field (separatrix). The discrepancy is mainly caused by neglecting the term $\vec{J}_e \times \vec{B}$ in the "thermalized potential". It should be pointed out that thermalized potential model cannot be used in this region.

C. Effect of the complex magnetic field geometry. Non-uniform plasma density and temperature

In this section, a combined effect of magnetic field topology, plasma density, and electron temperature will be

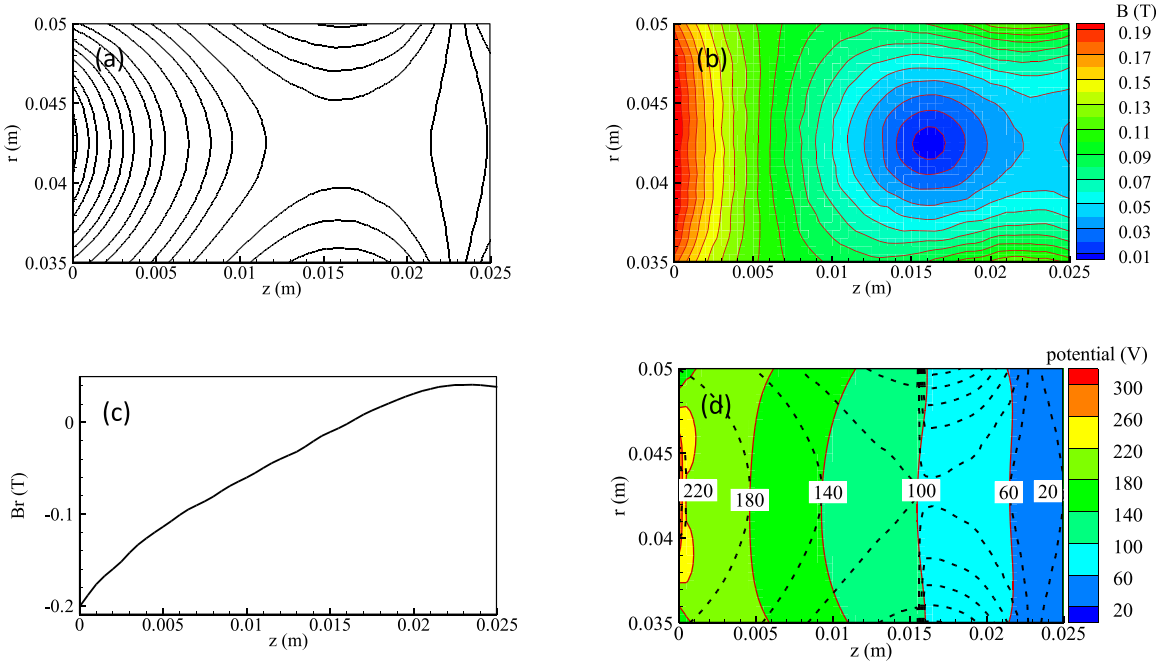

FIG. 5. Magnetic field and plasma potential distribution (Case 3): (a) magnetic field lines (Case 3), (b) magnetic field strength (unit: T), (c) Br along the channel centerline (Case 3), (d) comparison of equipotential contours of plasma potential with "thermalized potential" (black dashed lines).

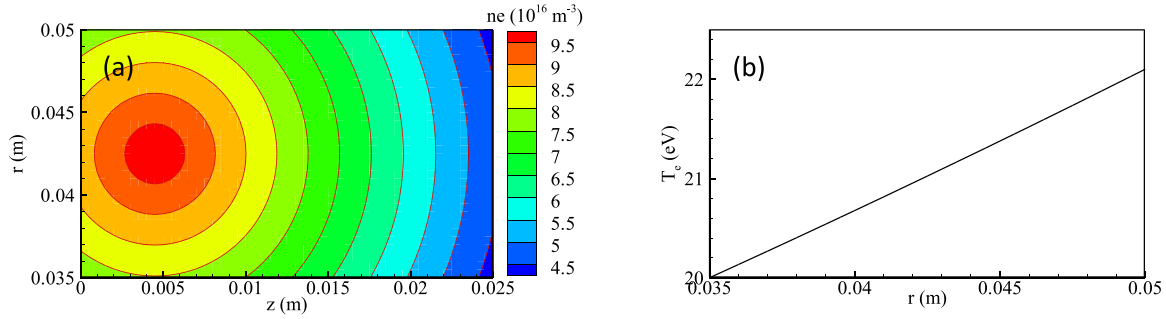

FIG. 6. Plasma density and temperature distribution: (a) plasma density distribution (10^{16} m^{-3}) and (b) plasma temperature distribution (eV).

described. Analysis of the plasma flow in the HT channel is performed using the hydrodynamic model of the plasma.[11] As a simplified representation of the flowfield in the thruster channel, the following distribution of plasma density and temperature shown in Fig. 6, which are similar to the results solved by hydrodynamic model of the plasma,[11] are employed in the analysis.

In this case, we consider three different shapes of the magnetic field distribution (corresponded to Cases 1–3 as shown in Figs. 3–5). The potential distributions solved by 2D solver and the thermalized potential are shown in Fig. 7.

It should be pointed out that the difference between the "thermalized potential" approach and generalized Ohm's law (i.e., Eq. (17) and Eq. (1)) is the term $\vec{J}_e \times \vec{B}$ which is neglected in Eq. (17). Generally, the electron current and the magnetic field are not parallel, especially in the non-uniform or complex fields and thus this term is non-zero. Therefore, strictly speaking the correct potential cannot be calculated using the "thermalized potential" approximation. This point has been demonstrated in Sec. IV.

It can be concluded that the axial magnetic component can cause the discrepancy between the equipotential contours calculated using the potential solver and that based on the "thermalized potential" model. Granted, the radial magnetic component is mostly dominant in the traditional HT channel, so the "thermalized potential" model can work very well. However, when the magnetic field topologies become complex (i.e., Bz/Br$> \sim 0.1$) in the advanced HT channel, like the magnetic in Figs. 4 and 5 (Cases 2 and 3), the "thermalized potential" model cannot accurately predict the potential distribution well. One reason is that the axial magnetic component is in the same order of magnitude to the radial magnetic component in some regions, the term $\vec{J}_e \times \vec{B}$ will not be negligible. Another reason is that the electron temperature is not constant along magnetic field lines, which is the important assumption for "thermalized potential."

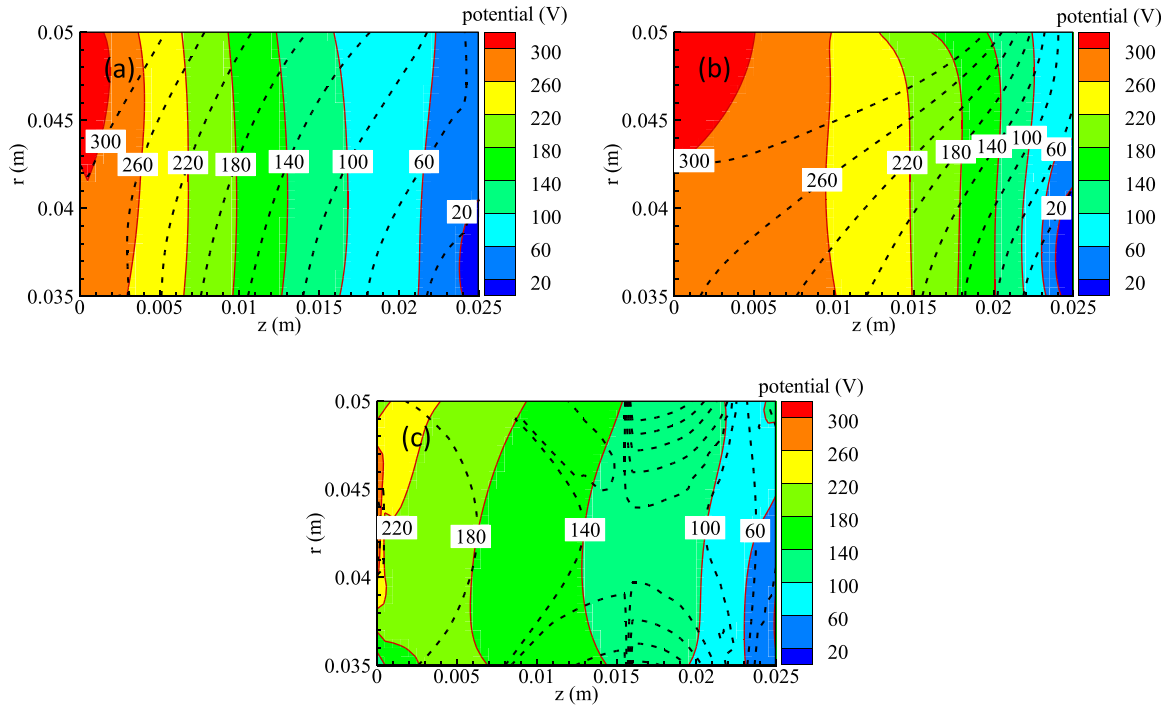

FIG. 7. Comparison of equipotential contours of plasma potential with "thermalized potential" (black dashed lines). (a) Case 1, (b) Case 2, (c) Case 3.

VI. CONCLUDING REMARKS

This paper aimed to analyze applicability of widely used assumption of "thermalized potential" and to define the "field of use" of application for this approach by analyzing various magnetic field topologies. Thermalized potential introduced by Morozov is a very useful concept simplifying solution of the plasma flow problem in magnetized plasma devices, such as HT, magnetrons, magneto-insulated diode, etc. However, applicability of this approach is limited to the cases in which magnetic field has relatively simple topology.

It can be concluded that the "thermalized potential" works very well when the magnetic field is nearly uniform and electron temperature is constant along the magnetic field lines. But if the magnetic field is highly non-uniform or the electron temperature is not constant along the magnetic field lines, the "thermalized potential" is not accurate. The reason is that the "thermalized potential" is based on the assumption that electron temperature is constant along the magnetic field and the term $\vec{J}_e \times \vec{B} = 0$. In some case with magnetic separatrix inside the thruster channel, when the assumption of constant electron temperature and the term $\vec{J}_e \times \vec{B} = 0$ cannot be satisfied, "thermalized potential" model cannot be applied at all. In those cases a full 2D potential solver must be applied.

ACKNOWLEDGMENTS

This work was supported in part by AFOSR (Dr. Mitat Birkan is the program manager). Authors also gratefully acknowledge the financial support from the China Scholarship Council.

[1]A. I. Bugrova, A. S. Lipatov, A. I. Morozov, and D. V. Churbanov, Tech. Phys. Lett. **28**, 821 (2002).
[2]A. Bouchoule, Ch. Philippe-Kadlec, M. Prioul *et al.*, Plasma Sources Sci. Technol. **10**, 364 (2001).
[3]A. I. Bugrova, A. I. Morozov, A. S. Lipatov *et al.*, in Proceedings of the 28th International Electric Propulsion Conference, Toulouse, France, 17–21 March 2003, Paper No. IEPC-03-366.
[4]L. Garrigues, G. J. M. Hagelaar, J. Bareilles, C. Boniface, and J. P. Boeuf, Phys. Plasmas **10**, 4886 (2003).
[5]A. Morozov and V. Savel'ev, Plasma Phys. Rep. **26**, 219 (2000).
[6]Y. Raitses and N. J. Fisch, Phys. Plasmas **8**, 2579 (2001).
[7]M. Martínez-Sánchez and E. Ahedo, Phys. Plasmas **18**, 033509 (2011).
[8]I. G. Mikellides, I. Katz, R. R. Hofer, D. M. Goebel *et al.*, Phys. Plasmas **18**, 033501 (2011).
[9]M. Keidar, A. D. Gallimore, Y. Raitses, and I. D. Boyd, Appl. Phys. Lett. **85**, 2481 (2004).
[10]A. I. Morozov, Y. V. Esinchuk, G. N. Tilinin *et al.*, Sov. Phys. Tech. Phys. **17**, 38 (1972).
[11]M. Keidar, I. D. Boyd, and I. I. Beilis, Phys. Plasmas **8**, 5315 (2001).
[12]V. V. Zhurin, H. R. Kaufman, and R. S. Robinson, Plasma Sources Sci. Technol. **8**, R1 (1999).
[13]I. D. Boyd, L. Garrigues, J. Koo, and M. Keidar, in Proceedings of 36th AIAA Joint Propulsion Conference, Huntsville, AL, 2000, Paper No. AIAA-2000-3520.
[14]G. J. M. Hagelaar, J. Bareilles, L. Garrigues, and J.-P. Boeuf, J. Appl. Phys. **91**, 5592 (2002).
[15]K. Komurasaki and Y. Arakawa, J. Propul. Power **11**, 1317 (1995).
[16]J. W. Koo, in Proceedings of the 42nd AIAA/ASME/SAE/ASEE Joint Propulsion Conference, Sacramento, CA, 9–12 July 2006, Paper No. AIAA 2006–4832.
[17]C. L. Ellison, Y. Raitses, and N. J. Fisch, Phys. Plasmas **19**, 013503 (2012).
[18]D. M. Young, Ph.D. dissertation, Harvard University, Cambridge, 1950.
[19]J. M. Fife and M. Martinez-Sanchez, in Proceedings of the 24th International Electric Propulsion Conference, Moscow, Russia, 19–23 September 1995, Paper No. IEPC-95-240.
[20]J. T. Yim, Ph.D. dissertation, The University of Michigan, Ann Arbor, 2008.
[21]D. Meeker, FEMM sofware version 4.2, 2008.